EUROPEAN SYNCHROTRON RADIATION FACILITY

INSTALLATION EUROPEENNE DE RAYONNEMENT SYNCHROTRON

Experiment Report Form

	Experiment title: Characterization of TiO2@YAG:Ce optical nanoparticles for solid state lighting applications	**Experiment number**: A26-2-907
Beamline: BM26	**Date of experiment**: from: 12 November 2018 to: 13 November 2018	**Date of report**: Sept 2022
Shifts: 3	**Local contact(s)**: BRUNELLI Michela	*Received at ESRF:*

Names and affiliations of applicants (* indicates experimentalists):

Maryam Yazdan Mehr, Delft University of Technology, EEMCS Faculty, Delft, The Netherlands

Abbas Bahrami, Delft University of Technology, EEMCS Faculty, Delft, The Netherlands

Willem van Driel, Delft University of Technology, EEMCS Faculty, Delft, The Netherlands

Report:

Aim of the project

Improving the efficiency and enhancing the colour uniformity of the LED-based products is one of the main goals of the lighting industry. Given that a significant share of worldwide energy consumption belongs to the lighting sector, any improvement in the performance and efficiency of LEDs will have a major positive implication for the society and the environment. This project aimed at synthesizing SiO_2-YAG:Ce^{3+} phosphor core-shell structures in order to increase the mie-scattering of the light and to increase the efficiency of LEDs. This will also result in products of higher reliability and lifetime. When it comes to the mie-scattering, the surface structure of particles (in this case SiO_2) and the uniformity of the shell thickness play a vital and prominent role. Not much is known about the kinetics and growth mechanism of the shell layer on SiO2 particles, and how this can be controlled and manipulated during synthesis. Direct microscopic methods are not suitable for this purpose, due to the fact that the shell is only a few nanometres. Small angle X-ray scattering (SAXS) technique is the most suitable method for studying the structure and the thickness of the YAG:$Ce3^{+}$ phosphor layer.

Materials and methods

YAG:Ce synthesis

YAG:Ce phosphor was synthesized by a novel simple method, wherein the mixture of three raw materials (Y2O3, Al2O3 and CeO2) were first acidified by diluted nitric acid to prepare a precursor, followed by a high temperature heating treatment of the obtained precursor under reductive atmosphere.

Synthesis of SiO_2@YAG:Ce core-shell phosphors

SiO_2 core spheres with YAG:Ce shell were prepared by a sole gel process. The starting materials were mixed in stoichiometric proportion. Materials were dissolved in dilute nitric acid solution. The prepared precursors were mixed with different ratios of water/ethanol solution containing citric acid as the chelating agent of the metal ions. The molar ratio of metal ions to citric acid was 1:2. Then, polyethylene glycol was added rapidly into the solution beaker with a concentration of 0.10 g/ml. The pH of the solution was adjusted ~6 and the solution was stirred for ~3 h to form sols. Then the silica particles were added under vigorous stirring. After being mixed for about 5 h, the suspension was separated by centrifugation. The particles were dried at 100˚C and annealed at the desired temperatures, for 2 h, with a heating rate of 4˚C/min. The above process was repeated several times to increase the thickness of the nano-layers on silica spheres. Due to a smooth and adherent formation of YAG:Ce^{3+} nano layers, coated on the silica spheres, the luminescence properties are comparable to that of the pure YAG:Ce3+ phosphors. Besides, SiO2 particles act as scattering agents in LED lens. Synthesized particles will then have dual functionalities, with superior photoluminescence properties and better colour temperature. Figure 1 shows schematics of a core-shell particle.

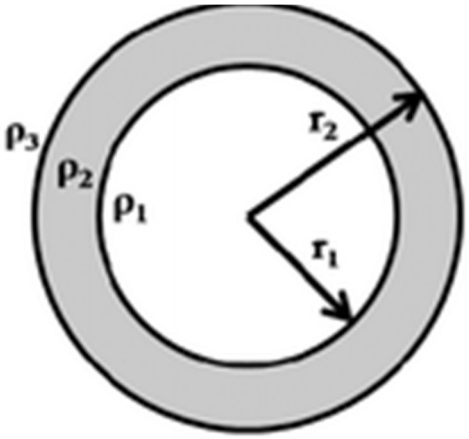

Figure 1: Core shell structure

SAXS Measurements

SAXS technique was carried out at ESRF to study the structural properties of particles, synthesized under various reaction conditions. This information can hardly be obtained with direct observation methods, including SEM and TEM. Data need to yet analysed, but we expect that SAXS provides information about aggregation, the thickness of shell, shell structure, particle size, and morphology. SAXS information can be obtained by plotting I(q) versus q function. The scattering curve, I(q), comes from the subtraction of the buffer from the sample, in which I(q) is a function of the momentum transfer and q is given as bellow:

$q=(2\pi \sin\theta)/\lambda$ (Å-1, nm-1)

Figure 2 shows SAXS set-up at ESRF in which detectors, and sample holders are clearly seen.

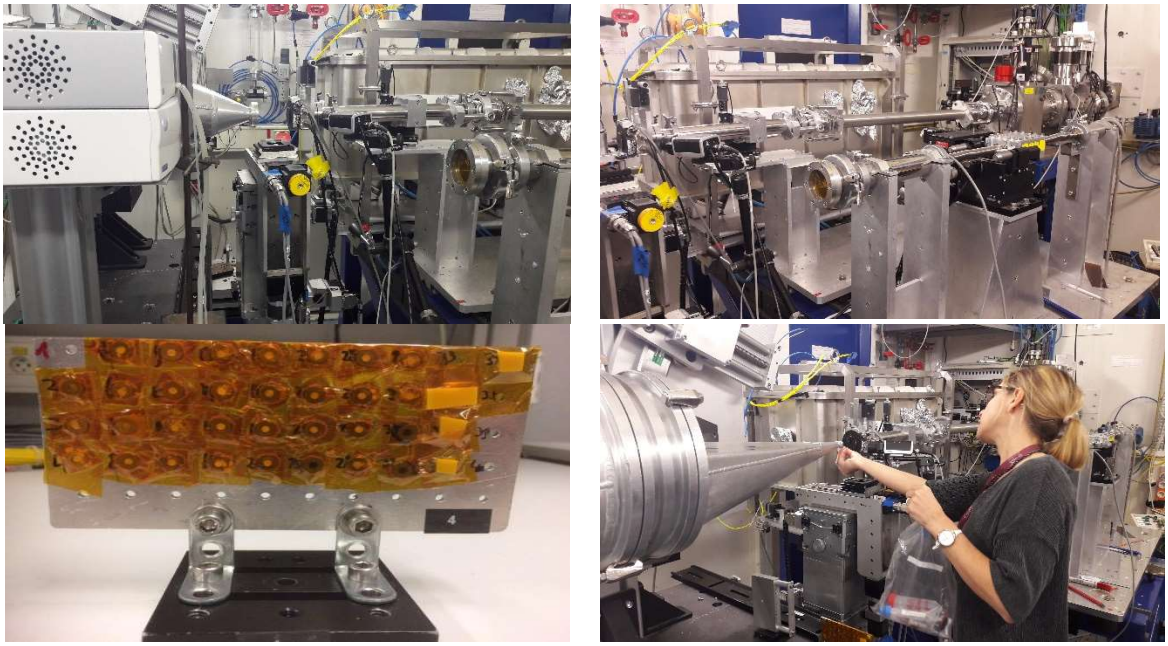

Figure 2: Small Angle X-ray Spectroscopy (SAXS) set-up at ESRF.

Almost two shifts were spent to set and optimize measurement parameters. The whole overnight was then devoted to do measurements on samples. WAXS data was also collected, since we realized that samples show good crystallinity (see diffraction rings of sample in position 3, Figure 3).

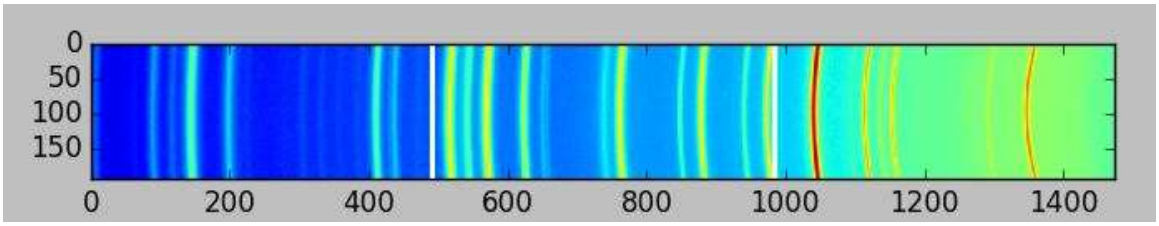

Figure 3: Crystallinity in samples.

Both SAXS and WAXS data were collected simultaneously, with same collection strategy that was collecting 8 images of 25 seconds each on all of the samples on the grid. Incoming wavelength of the x-ray beam was: ƛ= 1.040A. Data were azimuthally integrated in q space (unit nm-1), and subtracted the empty Kapton foil data as background.

Analyses of synthesized phosphor powders

The XRD patterns of as-prepared phosphor powders, synthesized at different pH values and calcined at 1000 °C for 4 h, are shown in Figure 4. It appeared the outcome of the synthesis was largely dependent on the pH values. The optimum synthesis condition is achieved when the pH is strictly controlled at a value of 3. Any deviation from pH=3 towards higher values, and more specifically towards ~3.5-4.0 pH range results in the appearance of YAM ($Y_4Al_2O_9$) and YAP ($YAlO_3$) transitional phases in as-synthesized powders. Figure 4 shows clear difference between XRD patterns of phosphor powders, synthesized at pH=3 and that synthesized at pH range 3.5-4. Boukerika *et al.* [1] reported that pure cubic YAG phase with optimum optical properties can be attained at pH≤4. It is reported that in case of pH≥6, the formation of unfavorable phases such as $Y_4Al_2O_9$ (YAM) and $YAlO_3$ (YAP) is inevitable. The finding in this study is rather different with what is reported by Boukerika *et al.* [1], as the pure YAG was found out to be obtainable at pH≤3. This has possibly to do with the fact that different raw materials are used in these studies. Both YAM and YAP phases are considered as impurities in YAG, as they cause energy level splitting of luminescence centers. This obviously adversely affects optical properties of phosphor. Overall, pH value appears to be the most crucial controlling factor when it comes to the final phase composition of synthesized powders. Obtaining a pure homogenous phosphor phase is only possible when pH is strictly controlled. As mentioned earlier, the pH in this case was kept at 3 by dropwise addition of NH_3 solution. Figure 4b also shows FESEM image of synthesized YAG:Ce powders. It is clear that nanoparticles

with spherical morphology are perfectly homogenously dispersed. Elemental mapping of a synthesized YAG:Ce particle, depicted in Figure 5, shows that elements are also perfectly homogeneously distributed.

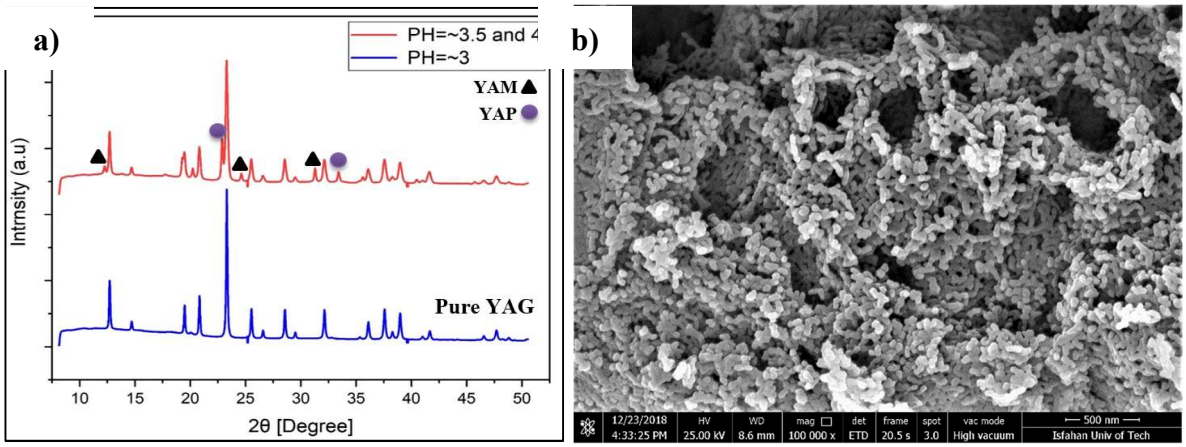

Figure 4. (a) XRD patterns of YAG:Ce nanoparticles, synthesized using solutions with different pH values and (b) FESEM image of synthesized YAG:Ce powders.

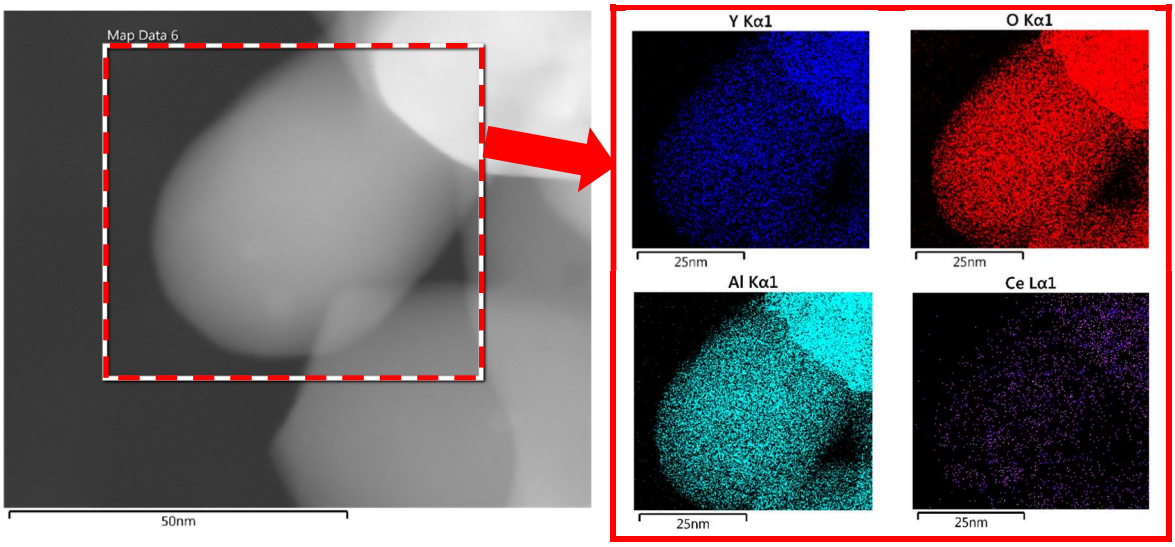

Figure 5. Elemental mapping of a YAG:Ce nanoparticle.

Figure 6a shows an example of the XRD pattern of samples annealed at 1000 °C. All peaks in the XRD patterns perfectly match with those of cubic YAG (JCPDS Card No. 79-1891) and no other crystalline phase such as $YAlO_3$ (YAP) or $Y_4Al_{12}O_9$ (YAM) can be detected. Also, to make sure that synthesized YAG has a structure, similar to that of industrial YAG, XRD spectra of synthesized and commercial YAG samples were compared (see Figure 6a). As mentioned earlier, single-phase pure YAG is very important to achieve high luminescence efficiency. Existing dopants obviously do not alter the structure of crystalline YAG. However, they surely change lattice parameters owing to the inequality of ionic radii between substituted yttrium ion and the dopant. A detailed XRD study on the effect of annealing time on the formation of YAG phase in core shell nanoparticles was carried out. Figure 6b shows XRD patterns of SiO_2@YAG:Ce nanoparticles after annealing from 1 to 10 h. The YAG phase starts to form after 1 h of annealing at 1000 °C. Therefore, one can conclude that crystallization time can be efficaciously decreased through the sol-gel method, so in this work the minimum crystallization time is found to be 1 h at 1000 °C. Appearance of sharp peaks and increasing the intensity of the main peak (2θ=33.4 is the point that cubic YAG:Ce structure main peak exist and related to the plane of crystalline with Miller indices of {4 2 0}) is an indication of crystallization during annealing. With the increase in calcination time, the intensity of diffraction peaks of SiO_2@YAG:Ce sample slightly increases, inferring that the degree of crystallinity has increased. Meanwhile, this also indicates that mean crystallite size increases with increase in annealing temperature. The same is expected when annealing temperature is increased. Figure 6c shows schematic view of crystal structure of YAG, showing that YAG has a cubic garnet structure, containing

octahedra (AlO_6), tetrahedra (AlO_4), and dodecahedra (YO_8) with corner-shared O atoms. The co-doped Ce^{3+} ion as luminescence centers substitutes for Y^{3+} ion that is located in the position of YAG dodecahedral.

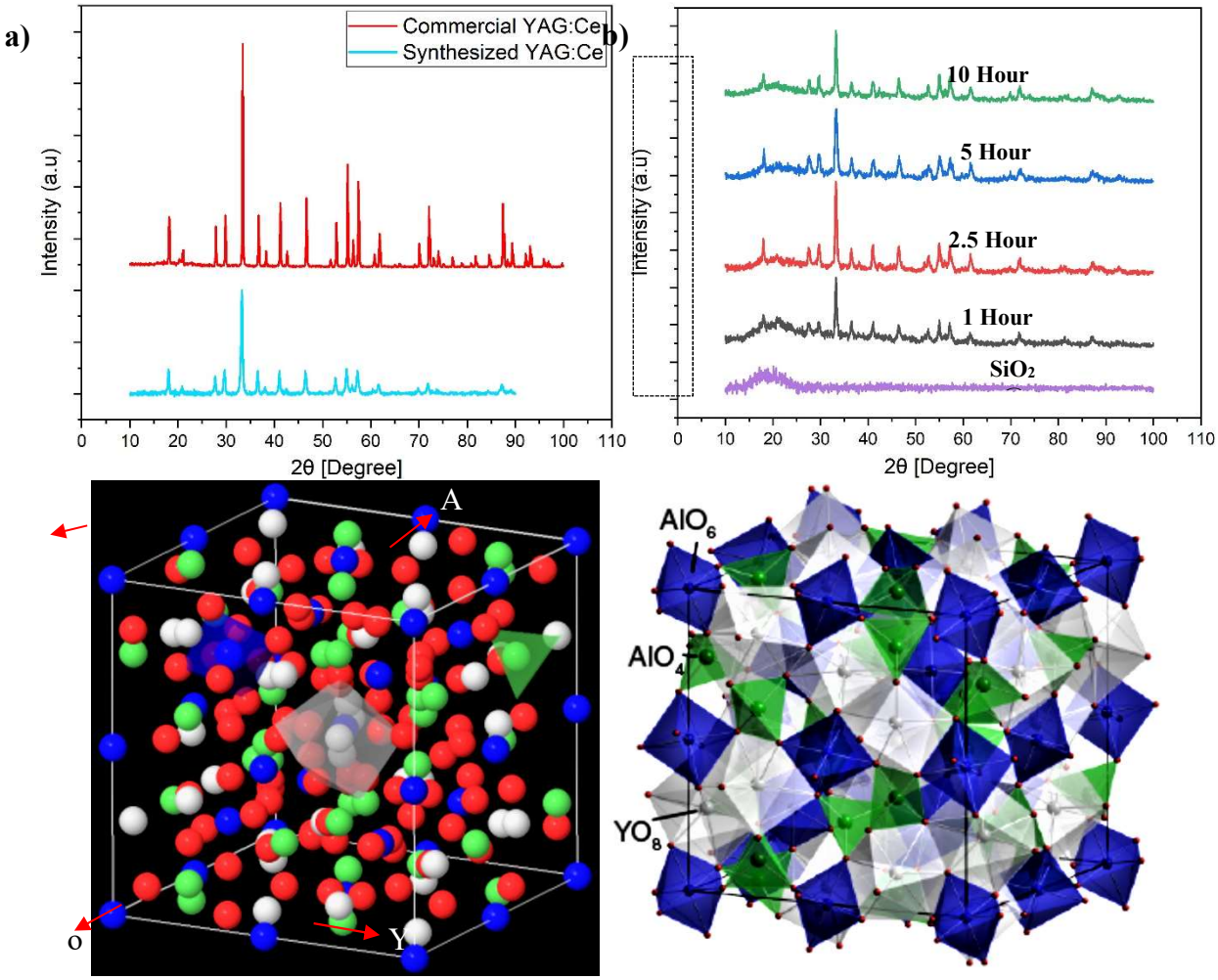

Figure 6. (a) X-ray diffraction patterns of synthesised YAG:Ce nanoparticles and commercial YAG:Ce (b) X-ray diffraction patterns of SiO_2@YAG:Ce nanoparticles after annealing, and (c,d) crystal structure of YAG [2].

SAXS analyses

Obtained SAXS data are presented in a log–log plot. SAXS curves are essentially plots of intensity as a function of the scattering vector $\boldsymbol{q}$, which corresponds to the scattering angle 2θ, given by [34]:

$$q = \left(\frac{4\pi}{\lambda}\right) \times \sin\theta \qquad (1),$$

The measured SAXS data were modeled using a commonly named global unified fit model [35,36]. In fact, this model includes a power-law regime in order to describe the mass or surface fractal and a Guinier regime for characterizing the mean structural size, given by:

$$I(q) = \sum_{i=1}^{n} \left[G_i \exp(-q^2 R_{gi}^2/3) + B_i \exp(-q^2 R_{g(i+1)}^2/3) \times \left\{ \frac{q}{\left[\mathrm{erf}\left(\frac{qR_{gi}}{\sqrt{6}}\right)\right]^3} \right\}^{-P_i} \right] \qquad (2),$$

where, R_{gi} is the radius of gyration, *erf* is written for the error function, i refers to the differently sized structures, G_i the Guinier pre-factor, and B_i is the pre-factor specific to the power-law scattering with an exponent P_i. The mean primary particle size d_p (for spherical particles) can be estimated from the radius of gyration R_g, which can be obtained by Guinier's law [35]:

$$d_P = 2\sqrt{\frac{5}{3}} \times R_g \qquad (3),$$

In case nanoparticles have a log-normal size distribution, in order to characterize the particle size distribution from the SAXS data, three fit parameters, *Rg*, *G and B* are often used. The geometric standard deviation (σ_g) in this case is given by [3]:

$$\sigma_g = \exp\left(\sqrt{\ln\frac{\left[B\times\frac{R_g^4}{1.62G}\right]}{12}}\right) \quad (4),$$

which characterizes the width of the size distribution. In the scattering vector q region, the scattering intensity *I(q)* can be characterized by the so-called power law [4]:

$$I(q) = B \times q^{-p} \quad (5),$$

where *B* is the power-law pre-factor and *P* refers to the power-law exponent. From log *I(q)* versus log q curves and slopes of linear region (at large values of scattering vector q), the values of the exponent *P* can be measured. In order to study particle surface characteristics like roughness, the surface-fractal dimension or d_s (d_s=6-P) is often used [2]. This is particularly useful for ideal two-phase structure with smooth surfaces and sharp boundaries.

In order to determine the effective thickness of boundary structure along the radial direction of the sphere (and more specifically for the spherical domain with a linear or sigmoidal electron-density interface gradient), the following formula can be used [3]:

$$E = 2\sqrt{3}\sigma \quad (6),$$

where σ is written for the standard deviation of the Gaussian smoothing function and *E* refers to the thickness of the diffuse boundary interface, which can be measured by [4]:

$$I(q) \approx K_p \times q^{-4} \times (1 - q^2E^2/12) \quad (7)$$

Figure 7a shows the scattering curves *I(q)* measured for pure SiO_2 and SiO_2@YAG:Ce nanoparticles. Before the coating was applied, the measured SAXS curve of un-coated SiO_2 did not exhibit any specific side maxima. In order to extract structural information from the spectra, the data of the pure SiO_2 were fitted by Guinier law (Eq. 2), the measured radius of gyration for primary particle of SiO_2 ($R_{G,P}$) is 8.9 nm (d_p= 22.97 nm, σ_g=1.34) which is in accordance with the presented TEM image. The power-law fit in the high of scattering vector q region follows Porod's law, *i.e.* $I \sim q^{-3.67}$, that implies these silica nanoparticles have almost smooth surfaces (surface fractals or D_s = 2.33). After preparation of core-shell nanoparticles, a specific side maximum or a shoulder appears (red mark). On the other hand, the coating process resulted in the formation of a YAG:Ce shell, growing on the SiO_2 particle surface gradationally by heterogeneous nucleation. Similar side maximum or shoulders have been reported in the literature as particle−particle interactions (structure factor). SiO_2@YAG:Ce with two times coating (coat II), the progressive growth of shell is more visible in the SAXS in which the shoulder or specific side maximum is more clear (Fig. 7b), suggesting that the shell grows with time. So, the YAG:Ce shell becomes thicker and the side maximum or shoulder is shifted to smaller scattering vector q region. In order to calculate the shell thickness, the SAXS data of the pure SiO_2@YAG:Ce (coat I and II) were fitted by Eq. 7, as displayed in Figures 7a and 6b. The calculated mean thicknesses of the diffuse and formed interfacial boundary nanostructured layer of one and two cycle coating are 2.8 nm and 7.7 nm, respectively. The stability of SiO2@YAG:Ce core–shell nanoparticles at 1000 ºC for different time was investigated by heating the sample from 1 to 10 hour in air. Figure 8 shows SAXS measurement of SiO_2@YAG:Ce nanoparticles, calcined at 1000 ºC for different times. It is noticeable that SAXS curves for all the specimens is almost similar, inferring that after calcination the core–shell structure of SiO_2@YAG:Ce nanoparticles was perfectly preserved. Even heating the sample up to 10 h hardly results in any change in the morphology of nanoparticles, inferring that SiO_2 cores are still encaged within the YAG:Ce shells, obviously showing high thermal stability of SiO_2@YAG:Ce core–shell nanoparticles. It is noteworthy that the exponent of power-law fit at large q is greater than four (for example, $I \sim q^{-4.20}$), inferring that there exists a sprayed and formed boundary nanostructure like thin layer formed on the particle surface of SiO_2.

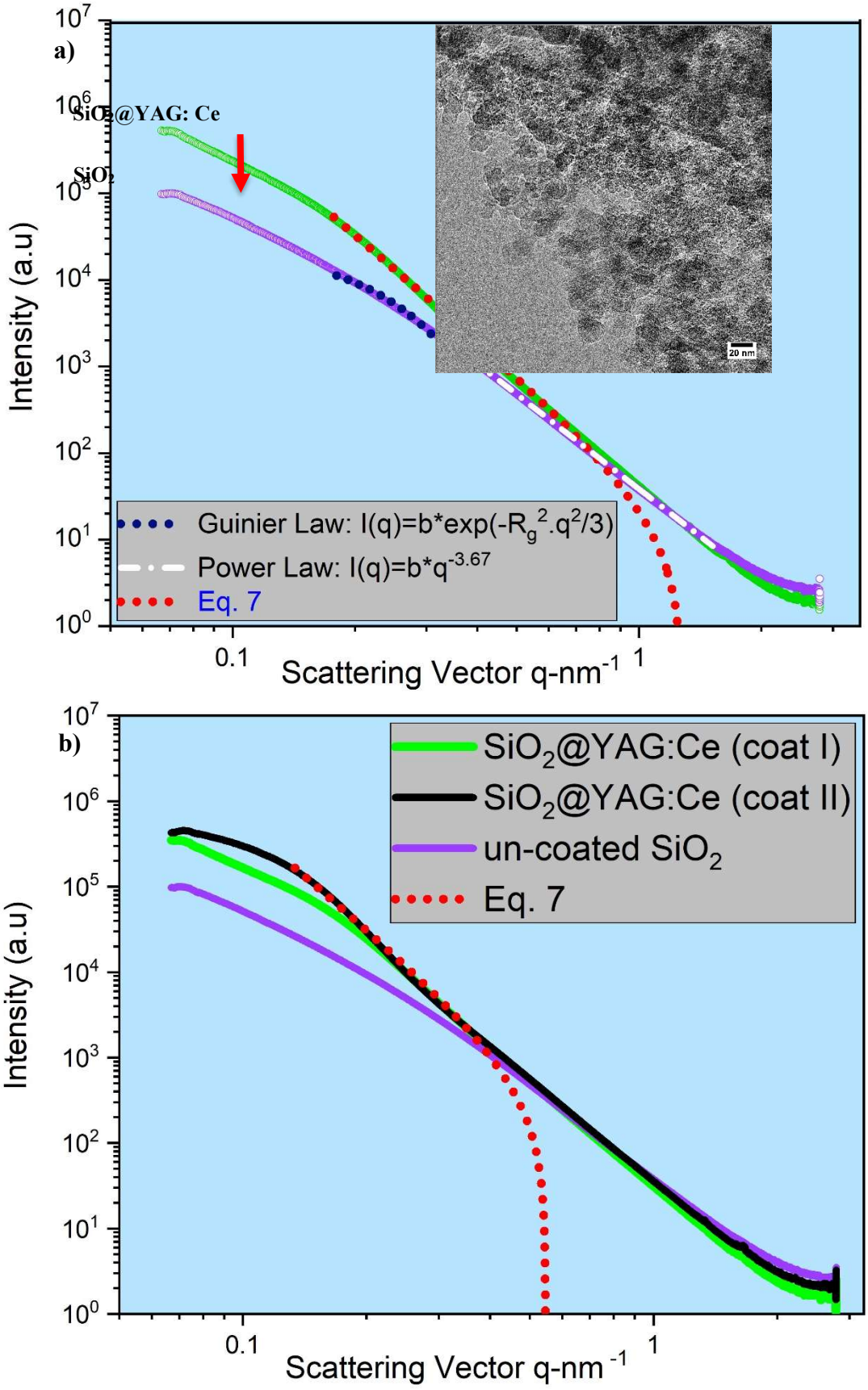

Figure 7. (a) SAXS curves of SiO_2 and SiO_2@YAG:Ce (b) SAXS curves of SiO_2 and SiO_2@YAG:Ce (coat I and II).

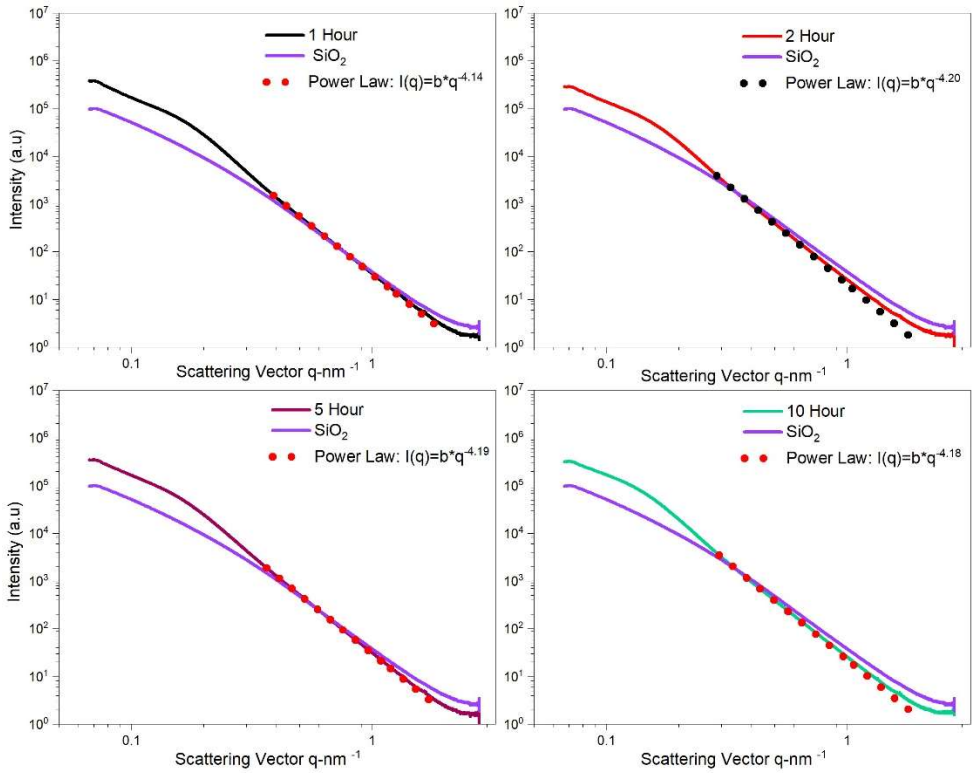

Figure 8. SAXS curves of core shell nanoparticle calcined at 1000 °C for different times.

Conclusions:

This paper investigates the synthesis, structure, and optical properties of multi-functional SiO_2@YAG:Ce nanoparticles for solid state lighting applications. The following conclusions can be drawn:

- Results showed that the final phase composition of synthesized powders largely depends on the pH values. The optimum synthesis condition is achieved when pH is strictly controlled at - Any deviation from pH=3 towards higher values, and more specifically towards ~3.5-4.0 pH range results in the appearance of YAM ($Y_4Al_2O_9$) and YAP ($YAlO_3$) transitional phases in as-synthesized powders, with both having adverse attribution to the optical characteristics of YAG:Ce powders.

- SAXS analysis showed that the mean thicknesses of YAG:Ce shell after one and two coating cycles were 2.8 nm and 7.7 nm. This was further confirmed by HRTEM direct observations.

- Heating the sample up to 10 h hardly results in any change in the morphology of nanoparticles, inferring that SiO_2 cores are still encapsulated by YAG:Ce shell, obviously showing perfect thermal stability of SiO_2@YAG:Ce core–shell nanoparticles.

- SiO_2@YAG:Ce (1.0 at.% Ce) core-shell nanoparticles show the highest emission, compared to commercial and synthesized YAG:Ce/SiO_2 mixture composite.

- The number of coating cycles play a vital role in enhancing the PL intensity of the core-shell particles. The increase in the PL intensity with double coating cycle is obviously attributable to the increase of the shell thickness (YAG:Ce) on the SiO_2 cores which in turn increases emitting ions (Ce^{3+}) per core–shell particle.

Acknowledgement:

The SAXS experiments were performed on beamline DUBBLE (beam number 26-02-894 and file number 195.068.1155) at the European Synchrotron Radiation Facility (ESRF), Grenoble, France. We are grateful to Local Contact at the ESRF for providing assistance in using beamline DUBBLE. Authors would also like thank Netherlands Organisation for Scientific Research (NOW) for support in doing SAXS experiments.

References:

[1] Selim, F.A.; Khamehchi, A.; Winarski, D.; Agarwal, S. Synthesis and characterization of Ce:YAG nano-phosphors and ceramics. *Opt. Mater. Express* **2016**, *6*, 3704.

[2] Boukerika, A.; Guerbous, L.; Brihi, N. Ce-doped YAG phosphors prepared via sol-gel method: Effect of some modular parameters. *J. Alloys Compd.* **2014**, *614*, 383–388.

[3] Garnet - Y3Al5O12 — ChemTube3D Available online: https://www.chemtube3d.com/ss-ygarnet/ (accessed on Oct 8, 2019).

[4] Gutsche, A.; Meier, M.; Guo, X.; Ungerer, J.; Nirschl, H. Modification of a SAXS camera to study structures on multiple scales. *J. Nanoparticle Res.* **2017**, *19*.